Arabian Journal of Chemistry (2023) **16**, 105016

King Saud University

Arabian Journal of Chemistry

www.ksu.edu.sa
www.sciencedirect.com

ORIGINAL ARTICLE

Study on ultrasonic depolymerization of Si-Ge precipitation in zinc oxide dust leaching process

Lei-ting Song [a,b,c], Hao-kai Di [a,b,c], Ming liang [a,b,c], Yin-er Zeng [a,b,c], Kun Yang [a,b,c,*], Li-bo Zhang [a,b,c,*]

[a] *State Key Laboratory of Complex Nonferrous Metal Resources Clean Utilization, Kunming University of Science and Technology, Kunming, Yunnan 650093, China*
[b] *Yunnan Provincial Key Laboratory of Intensification Metallurgy, Kunming, Yunnan 650093, China*
[c] *Faculty of Metallurgical and Energy Engineering, Kunming University of Science and Technology, Kunming, Yunnan 650093, China*

Received 27 November 2022; accepted 16 May 2023
Available online 22 May 2023

KEYWORDS

Silicon germanium;
Polymerization precipitation;
Silicic acid colloid;
Ultrasonic depolymerization;
Mechanism

Abstract Under the background of the increasing demand for germanium in high-tech, this paper finds out the mechanism of silicon germanium polymerization precipitation by simulating the leaching process of zinc oxide dust containing germanium. By comparing and analyzing the simulation experiments under ultrasonic and conventional conditions, the mechanism of efficient dispersion and depolymerization of germanium silicon precipitation induced by ultrasonic was found out. The results show that in the leaching process of germanium-containing zinc oxide dust, due to the increase of local pH, some silicon ions in the solution will hydrolyze and polymerize to form silicic acid colloid to adsorb germanium in the solution, causing the loss of germanium 14.81%, resulting in low recovery rate of germanium industry. Ultrasonic wave was introduced in the leaching process, and the shock wave and micro-jet released by ultrasonic cavitation continuously impacted the surface of polysilicate colloid. The germanium adsorbed on the surface of the silicic acid colloid is desorbed, and the large particles of silica gel are depolymerized into small particles of silicic acid, which reduces the adsorption of silica gel on germanium. The loss of germanium under ultrasonic conditions can be reduced by 59.35%. This study can effectively realize the efficient recovery of germanium in zinc oxide dust, and provide process and theoretical basis for the sustainable development of germanium industry.

* Corresponding authors.
E-mail addresses: truepsyche@sina.com (K. Yang), zhanglibopaper@126.com (L.-b. Zhang).
Peer review under responsibility of King Saud University.

Production and hosting by Elsevier

https://doi.org/10.1016/j.arabjc.2023.105016

1. Introduction

As a multi-functional strategic metal resource, germanium is playing an increasingly important role in national defense science and technology, electronic optical fiber communication, medicine, aerospace, infrared optical materials, semiconductors and other fields with the development of science and technology(Zhang et al., 2018; Huang et al., 2022; Xiaodong and Feiyan, 2018; Ting et al., 2015; Dass, 2019). In recent years, with the development of high-tech industries such as global infrared optics and communication industries, the demand for germanium has been increasing. Studying the efficient extraction of germanium resources is of great significance for promoting Chinese scientific and technological progress and ensuring national defense security(Ting et al., 2015; Geng et al., 2022).

Chinese germanium production accounts for more than 65% of the world's total output, of which more than 70% comes from zinc oxide dust(Jikun and Aiping, 2005; Zhengwei et al., 2015). The content of germanium in dust is very low, generally 500–2000 g/t(Li et al., 2017; Zhang et al., 2019). At present, the two-stage counter-current acid leaching process is mainly used for the extraction of germanium from zinc oxide dust(Bo-kang and Yang, 2007; Yanlin et al., 2021). However, industrial practice shows that the recovery rate of zinc and germanium in the traditional two-stage counter-current acid leaching process is generally low, and the leaching rate of germanium is generally about 60–80%(Likun, 2020; Chunfu et al., 2021). In order to extract germanium from zinc oxide dust containing germanium more efficiently, researchers have done a lot of work. Deng et al. used one-stage atmospheric oxygen-rich leaching-neutralization process(Yingxu et al., 2021) and two-stage atmospheric oxygen-rich high-temperature leaching process(Zhigan et al., 2020) to treat germanium-containing zinc oxide dust. The leaching rates of germanium were 83% and 90%, respectively. In the above leaching process, the leaching rate of germanium will gradually decrease with the leaching time. The main component of zinc oxide dust containing germanium is zinc oxide. Zinc oxide has good hydrophobicity(Tarwal et al., 2023; Sutar et al., 2021; Patil et al., 2019) and will react to form zinc sulfate in sulfuric acid system. Therefore, the influence of zinc oxide can be excluded. Silica and silica-based hybrid nanoparticles can effectively adsorb impurities in water, so as to realize the treatment of sewage(Jadhav et al., 2019). Therefore, some scholars speculate that the decrease of germanium leaching rate in the process of dust leaching is caused by the influence of silicon(Song et al., 2022; Xu et al., 2023).

In order to eliminate the adverse effects of silicon on germanium leaching, researchers have put a lot of effort. For example, Harbuck (Harbuck, 1992; Harbuck, 1993) and Wang(Ji-min et al., 2014) used H_2SO_4-HF mixed acid to leach the replacement slag of zinc concentrate oxygen pressure acid leaching zinc smelting process. The results show that the leaching rate of germanium can reach more than 90%. However, due to the introduction of F^- in the leaching, it will have a serious impact on the subsequent electrowinning process, resulting in electrolytic sintering. LIU et al.(Liu et al., 2016) used high pressure acid leaching process to treat zinc powder replacement gallium germanium slag, the leaching rate of germanium can reach more than 94%, high pressure acid leaching can leach some insoluble substances. However, the equipment required for pressure acid leaching is complex, the investment and operating costs is high, and it is difficult to industrialize. Wang et al.(Wang et al., 2017) used microwave alkaline roasting-water soluble zinc oxide dust containing germanium, and the leaching rate of germanium increased from 80.35% to 91.15%. Microwave can improve the microstructure of the material and increase the leaching rate of germanium. However, microwave requires a large investment in equipment and is difficult to connect with industrial production. Liu et al.(Liu et al., 2016; Liu et al., 2017) also carried out the study of adding sodium dodecyl sulfate and oxalic acid to the sulfuric acid leaching system at atmospheric pressure. The leaching rate of germanium can reach more than 90%, but copper, lead and other elements will affect the complexation leaching of oxalic acid and germanium, and the introduction of organic salts is not conducive to the subsequent electrowinning process.

In recent years, ultrasound has attracted more and more attention from metallurgical workers due to its unique physical and chemical effects, and has been gradually cited in the field of hydrometallurgy (Yan et al., 2020; Wang et al., 2017). The "cavitation effect" will occur in the solution under the action of ultrasound, resulting in cavitation bubbles. The energy released when cavitation bubbles break, as well as the shock waves and micro jets formed, can damage the solid surface, which is conducive to the development of pore cracks and the formation of new reaction interfaces. Under conventional conditions, the coverings generated before and during the reaction of the solid phase will be destroyed under the action of ultrasound, thus exposing the fresh interface(Jordens et al., 2015; Li et al., 2014; Zhang et al., 2015). In this study, based on the composition analysis of the leaching solution of industrial zinc oxide dust, the formation mechanism of silicon–germanium precipitation in the leaching process of zinc oxide dust was investigated by pure solution simulation experiment, and the ultrasonic field was used to inhibit the aggregation and precipitation of silicon–germanium.

2. Experiments and methods

2.1. Experimental design

In order to study the precipitation mechanism of silicon and germanium in the leaching process, this study used a pure solution to simulate the dust neutralization leaching process (Yanlin et al., 2021). The composition of industrial zinc oxide dust leaching solution was analyzed by elemental quantitative analysis method, and the results are shown in Table 1. It can be found that the concentration of Zn, Ge and Si in the leaching solution of zinc oxide dust is 109.25 g/L, 51.35 mg/L and 49.49 mg/L, respectively. The chemical reagents required for this experiment are concentrated sulfuric acid, germanium dioxide, sodium silicate, sodium hydroxide, zinc oxide, and their purity is AR grade. In order to facilitate the study, only considering the influence of silicon and germanium, the concentration of the above Ge and Si is enlarged by 10 times, that is, the pure solution with Ge and Si concentrations of 0.5 g/L and sulfuric acid acidity of 30 g/L is configured for simulation experiments.

2.2. Experimental method

The ultrasonic equipment used in this experiment is shown in Fig. 1. The ultrasonic device involved in this experiment is a probe reactor, which has the advantage of high sound intensity(Zhaohui et al., 2010). The frequency of the ultrasonic device is 22 kHz, the total power is 1000 W, and the power can be adjusted with the experimental requirements. An appropriate amount of the configured pure solution was placed in a beaker and heated to 80 ℃ in a water bath. The zinc oxide slurry was added to the beaker, and the pH of the solution was adjusted to 2–3. After centrifugal separation, the centrifugal liquid and centrifugal slag were obtained. The centrifugal slag was dried in a drying oven and retained. The content of silicon and germanium in the centrifugal liquid was measured by elemental quantitative analysis method, and the loss rate of silicon and germanium was calculated. The main reactions

Table 1 The main chemical components of industrial zinc oxide dust leaching solution, g/L (* mg/L).

Composition	Zn	Ge*	Si*	H_2SO_4
Content	109.25 g/L	51.35 mg/L	49.49 mg/L	31.60 g/L

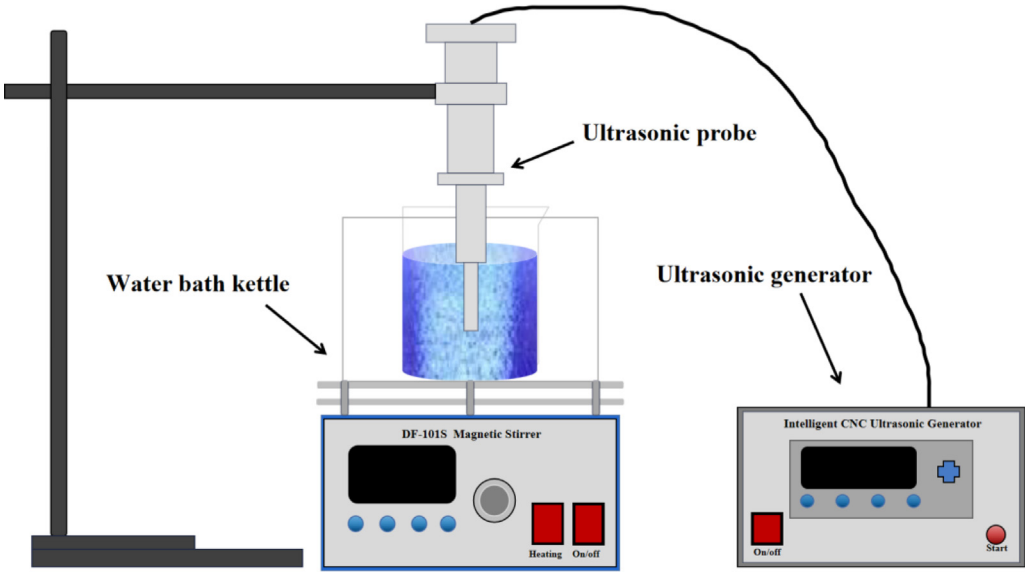

Fig. 1 Experimental device diagram.

involved in the simulation experiment are as follows(Markus et al., 2004):

$$ZnO + H_2SO_4 = ZnSO_4 + H_2O \quad (1)$$

$$Si^{4+} + 3H_2O = H_2SiO_3 + 4H^+ \quad (2)$$

The calculation method of germanium loss rate is as follows:

$$x = (1 - \frac{C_1 \times V_1}{C_0 \times V_0}) \times 100\% \quad (3)$$

Where x is the loss rate of silicon and germanium, %; C0 is the initial concentration of silicon and germanium in the simulated solution, g/L; C1 is the concentration of silicon and germanium in the centrifugal liquid, g/L; V0 is the volume of simulated solution, L; V1 is the volume of centrifugal liquid, L.

2.3. Characterization and analysis

Scanning electron microscopy (SEM, Zeiss Sigma 300, Germany) was used to analyze the surface element distribution and microstructure of the samples. The phase form of samples was detected by Raman spectrometer (HORIBA Scientific LabRAM HR Evolution, HORIBA, Villeneuve d'Ascq, France). The chemical composition fragments in the samples were analyzed by Time of Flight Secondary Ion Mass Spectrometry (TOF-SIMS 5 IONTOF, PHI NanoTOFII, UK). The pore size of the samples was determined by a specific surface area analyzer (BET, ASAP 2460 3.01, Micromeritics, US). The particle size and Zeta potential of samples were measured by nano particle size and Zeta potential analyzer (Malvern Zetasizer Nano ZS90, Malvern, UK).

3. Results and discussion

3.1. Experimental result

The loss rate of germanium in simulated solution under ultrasonic and conventional conditions is shown in Fig. 2. It can be seen that through the simulation experiment, the loss rate of germanium in the simulated solution is 14.81% in the conven-

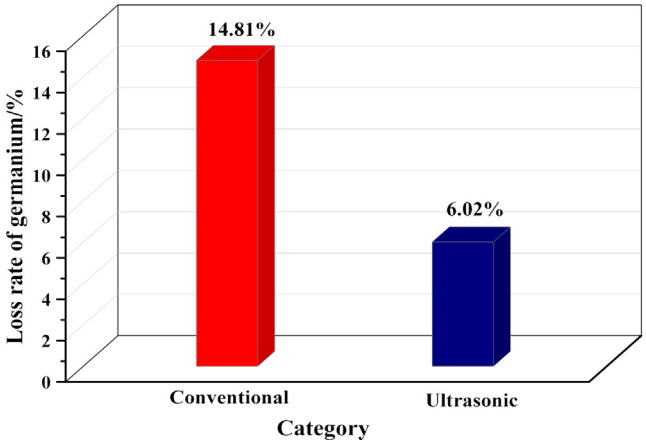

Fig. 2 The loss rate of germanium in simulated solution under ultrasonic and conventional conditions.

tional leaching process, while the loss rate of germanium in the simulated solution is 6.02% when the ultrasonic with a power of 500 W is introduced in the leaching process. The loss rate of germanium in simulated solution after ultrasonic treatment is 59.35% lower than that under conventional conditions. Through the simulation experiment, it can be seen that the reason of germanium loss may be due to the high local pH value of the solution in the leaching process, which leads to the hydrolysis of part of the silicon in the solution into silicic acid colloid, so as to adsorb the germanium leached in the solution, thus resulting in germanium loss. The introduction of ultrasonic waves during the leaching process can inhibit the loss of germanium.

3.2. Polymerization precipitation mechanism of silicon germanium

In order to explore the mechanism of silicon germanium polymerization precipitation in the leaching process, the above-mentioned dried centrifugal slag was analyzed by SEM and Raman spectroscopy, and the results were shown in Fig. 3 and Fig. 4.

Fig. 3 is the SEM element surface scan distribution of centrifugal slag. It can be found that the distribution of S in the four elements of S, O, Si and Ge are the most uniform, and the three elements of O, Si and Ge have obvious concentrated distribution. From the diagram, it can be seen that the concentrated distribution of Si and Ge is the closest. In the area where Si is concentrated, the distribution of Ge is often more concentrated. Therefore, it can be judged that the enrichment area of Si and Ge in the centrifugal slag is relatively consistent, which indicates that Si and Ge in the centrifugal slag exists together. It can indirectly prove that the loss of germanium in the solution is due to the formation of silica gel in the solution to adsorb it.

Fig. 4 is the Raman surface scan of the centrifugal slag. The Raman peak in the range of 260–300 cm^{-1} belongs to Ge-Ge bond(Lulu et al., 2016; Rouchon et al., 2014). The Raman peak in the range of 400–600 cm^{-1} is amorphous silicon, and there is Si-Si bond(Rouchon et al., 2014; Guohua et al., 1987). Therefore, according to the difference of the Raman peaks in the figure below, it can be judged that the red part is silicon Raman diagram and the blue part is germanium Raman diagram. It can be seen from the figure that the peak near 1040 cm^{-1} in silicon Raman belongs to the antisymmetric stretching vibration of Si-O-Si(Lu et al., 2015). The peak at 450–600 cm^{-1} in the germanium Raman peak can be attributed to the symmetric stretching vibration of Ge-O-Ge (Mochida et al., 1984). The Raman peak between 600 and 700 cm^{-1} is the vibration of the six-coordinate germanium

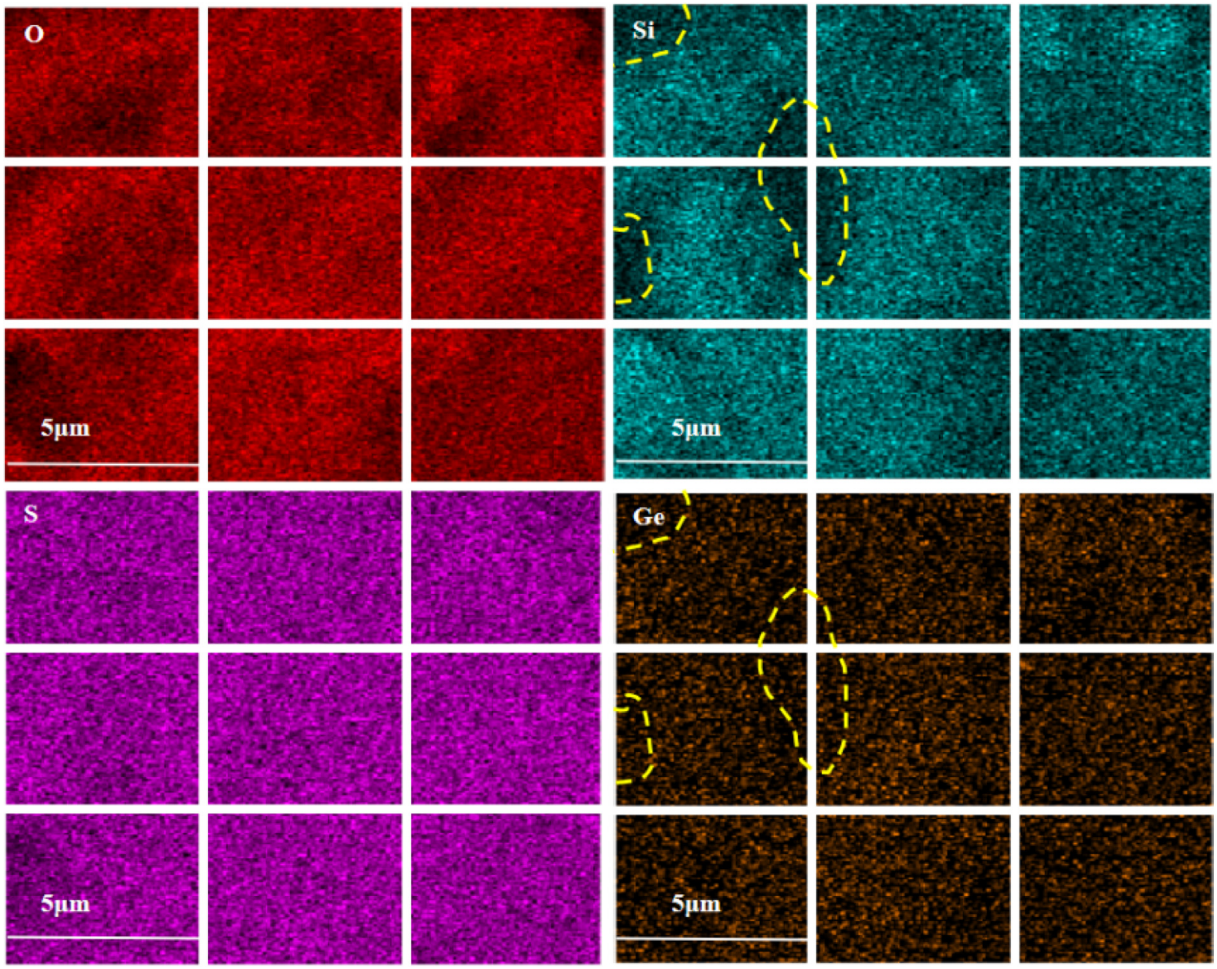

Fig. 3 SEM mapping element distribution of centrifugal slag.

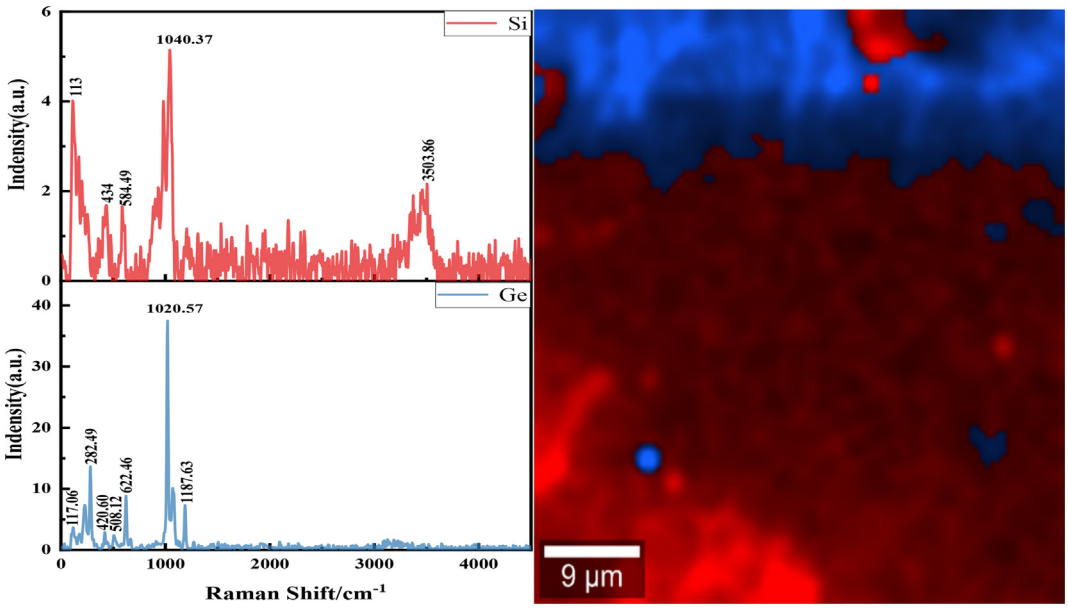

Fig. 4 Raman surface scan analysis of centrifugal slag.

group bridge oxygen(Verweij and Buster, 1979). According to the Raman peak diagram obtained by Raman scanning, it can be found that silicon exists in the form of silicic acid, and germanium in the precipitate exists in the form of germanic acid. From the Raman map, it can be seen that the silicic acid and germanium is wrapped and adsorbed together.

The centrifugal slag was analyzed by time-of-flight secondary ion mass spectrometry, and the results are shown in Fig. 5. TOF-SIMS can obtain the fragmentation information of the sample composition, which is complementary to the results of SEM and Raman scanning, and further verifies the conclusion that silicic acid colloid adsorbs germanium. From the following diagram, it can be found that there are HSO_4, SO_3, SiO_3H, SiO_2, Ge, GeOH and other fragments in the fragments of TOF-SIMS, among which SiO_2, SiO_3H and SiOH may be fragments of silicic acid molecules, GeO and GeO_3 are fragments of germanic acid molecules. It can be seen from Fig. 5 that the aggregation regions of silicon and germanium are basically the same, and the green Ge-Si standard isotope spectrum peak does not correspond to the detected spectrum peak, which indicates that no Ge-Si bond fragments are found in the TOF-SIMS analysis. Combined with the results of the

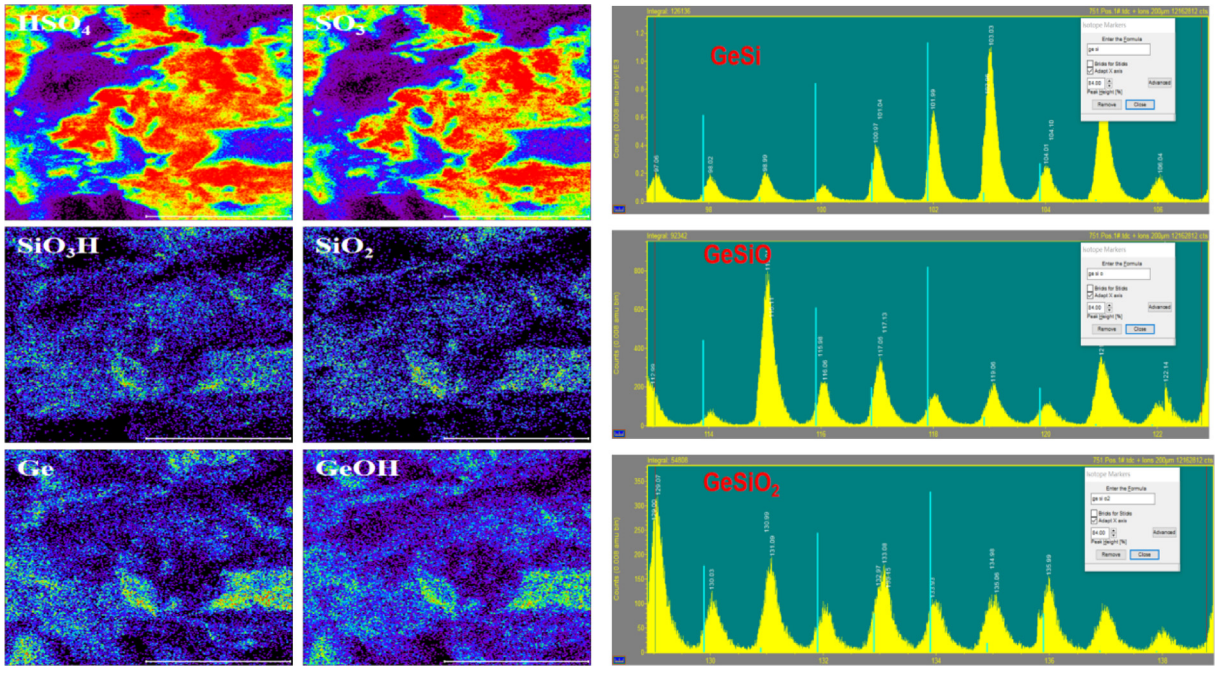

Fig. 5 TOF-SIMS analysis of centrifugal slag.

above SEM surface scan and Raman surface scan, it can be determined that the hydrolysis of silicon into silicic acid colloid absorbs germanium in the solution and causes the loss of germanium.

3.3. Ultrasonic induced dispersion depolymerization of silicon–germanium precipitation

In order to clarify the depolymerization effect of ultrasound on germanium adsorbed by silicic acid during leaching process, ultrasound with a power of 500 W was added during the stirring process of the simulated solution. The centrifugal slag and simulated solution under ultrasonic and conventional conditions was subjected to BET, particle size, Zeta potential, Raman, SEM and other comparative characterization analysis.

3.3.1. BET comparative characterization

The centrifugal slag under ultrasonic and conventional conditions was analyzed by BET, and the analysis results were shown in Fig. 6. It can be found from Fig. 6 that the pore size of centrifugal slag under conventional conditions is mainly distributed between 5 and 50 nm, which belongs to mesoporous pore. The pore size of centrifugal slag under ultrasonic conditions is mainly distributed between 50 and 350 nm, which belongs to macroporous pore(Marek, 2013). According to the BET simulation results, the specific surface area of the centrifugal slag under conventional conditions is 9.891 m^2/g, the pore size is 9.098 nm, and the pore volume is 0.038 cc/g. The specific surface area of the centrifugal slag under ultrasonic conditions is 15.647 m^2/g, the pore size is 69.720 nm, and the pore volume is 0.101 cc/g. The specific surface area, pore size and pore volume of centrifugal slag under ultrasonic conditions was 58.19 %, 666.32 % and 165.79 % higher than those under conventional conditions. This is caused by the jet and cavitation generated by ultrasound. The jet generated by ultrasound will continuously impact the surface of silicic acid colloid, peel the germanium adsorbed on its surface, and expand the pore size. Combined with the high temperature and high pressure generated by cavitation, the pore size of centrifugal slag under ultrasonic conditions will be further expanded, and the pore volume and specific surface area will be increased.

3.3.2. Comparative characterization of nano-particle size and Zeta potential

The particle size and Zeta potential of simulated solutions with different pH under ultrasonic and conventional conditions was analyzed. The results are shown in Fig. 7 and Fig. 8. The left and right sides of Fig. 7 are the particle size distribution of the solution under conventional and ultrasonic conditions. It can be seen from Fig. 7 that the particle size in the solution increases from 2.62 nm to 751 nm with the increase of the pH of the solution under conventional conditions, and the particle size in the solution increases from 3.24 nm to 157 nm with the increase of the pH under ultrasonic conditions. This shows that with the increase of the pH of the solution, the silicon in the solution will be hydrolyzed and adsorbed germanium, and aggregation will occur, resulting in an increase in the particle size of the solution. Moreover, when the pH is 3, the particle size of the simulated solution under ultrasonic conditions is much smaller than that of the conventional solution, which indicates that the ultrasound can effectively reduce the particle size during the leaching process, destroy the agglomeration of

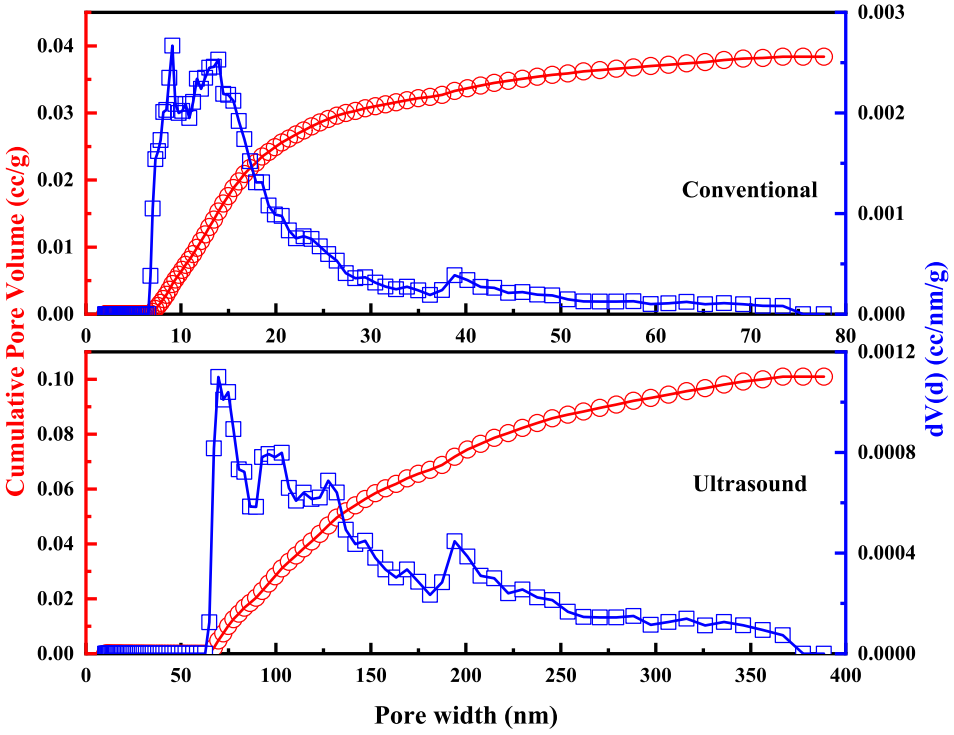

Fig. 6 Analysis of BET of centrifugal slag under ultrasonic and conventional conditions.

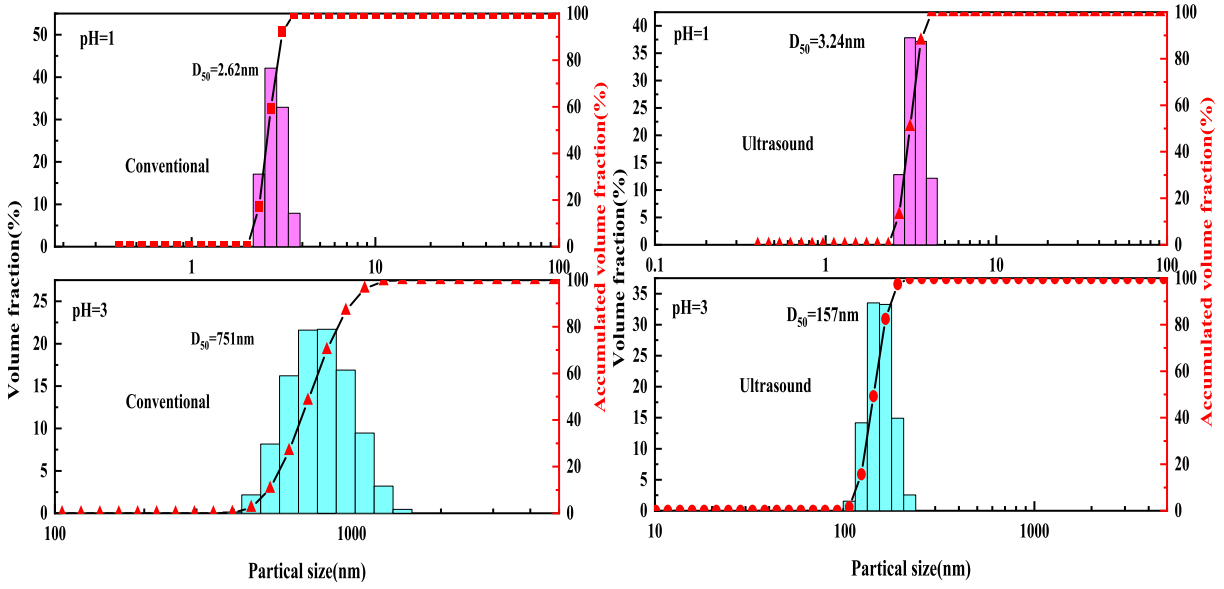

Fig. 7 Particle size distribution of simulated solutions with different pH values under conventional and ultrasonic conditions.

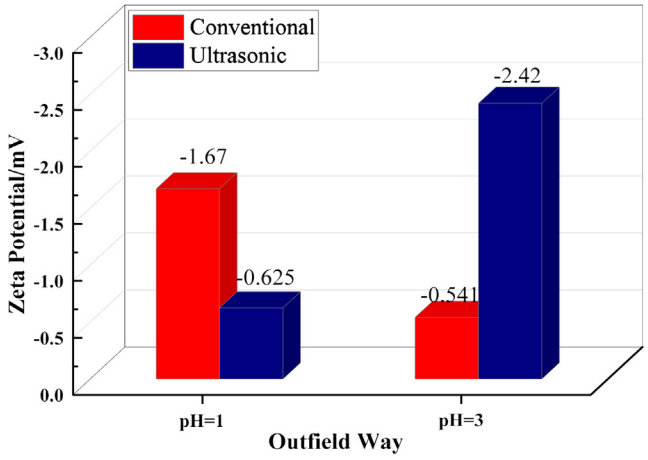

Fig. 8 Zeta potential of simulated solutions with different pH under conventional and ultrasonic conditions.

the silicic acid colloid, depolymerize the large particles of silica gel into small particles of silicic acid molecules, and effectively inhibit the aggregation of the silicic acid colloid.

The Zeta potential is an important index to characterize the colloidal dispersion system. The absolute value of the Zeta potential represents the stability of the colloidal dispersion system. The lower absolute value of Zeta potential indicates that the colloid is more likely to agglomerate.. Fig. 8 is the Zeta potential diagram of the simulated solution at different pH under ultrasonic and conventional conditions. It can be found from Fig. 8 that under the condition of pH = 1, the Zeta potential of the solution under conventional and ultrasonic treatment methods is −1.67 mV and −0.625 mV, respectively. The absolute value of Zeta potential under ultrasonic conditions is significantly smaller than that under conventional conditions. This is because the mechanical effect of ultrasound will accelerate the collision of local particles in the solution and easily agglomerate. As the pH increased to 3, the Zeta potential in the solution under conventional conditions was −0.541 mV, while the Zeta potential in the solution under ultrasonic conditions was −2.42 mV. This is because under normal conditions, with the increase of pH, more silicic acid colloids will be formed in the solution and agglomeration will occur more easily. Under ultrasonic conditions, due to the cavitation generated by ultrasound itself, agglomerated particles will be broken and the aggregation of colloids will be hindered. This is also consistent with the results of the above particle size.

3.3.3. Comparative characterization of Raman spectra

The peak with wave number of 900–1100 cm^{-1} in the Raman spectrum is attributed to the stretching vibration of silicon-oxygen tetrahedron (SiO_4^{i-}) in silica gel, and the silicon-oxygen tetrahedron with different bridging oxygen bonds has different Raman shifts(Tan et al., 2004; Zhang et al., 2021). In the Raman spectrum fitting curve of amorphous hydrated SiO_2, the peak near 950 cm^{-1} is attributed to the stretching vibration of silicon oxygen tetrahedron (Q1) with one bridge oxygen and three non-bridge oxygen. The peak near 980 cm^{-1} can be attributed to the silicon-oxygen stretching vibration of silicon-oxygen tetrahedron (Q2) with two bridged oxygen and two non-bridged oxygen. The peak near 1010 cm^{-1} is the silicon oxygen stretching vibration of silicon oxygen tetrahedron (Q3) with three bridge oxygen and one non-bridge oxygen. The peak near 1150 cm^{-1} is the stretching vibration of silicon-oxygen tetrahedron (Q4) containing four bridge oxygen atoms(Miao, 2020; Xinhao, 2022).

Raman spectral analysis was performed on centrifugal slag under ultrasonic and conventional conditions, and the results were shown in Fig. 9. It can be seen from the figure that the peak representing the stretching vibration of silicon-oxygen tetrahedron (SiO_4^{i-}) in silica gel under ultrasonic conditions is significantly smaller than that under conventional conditions. Under conventional conditions, the areas of Q3 and Q4 in the Raman spectral Gaussian diagram of centrifugal slag are 31.09% and 68.91%, respectively, while the areas of Q1, Q3

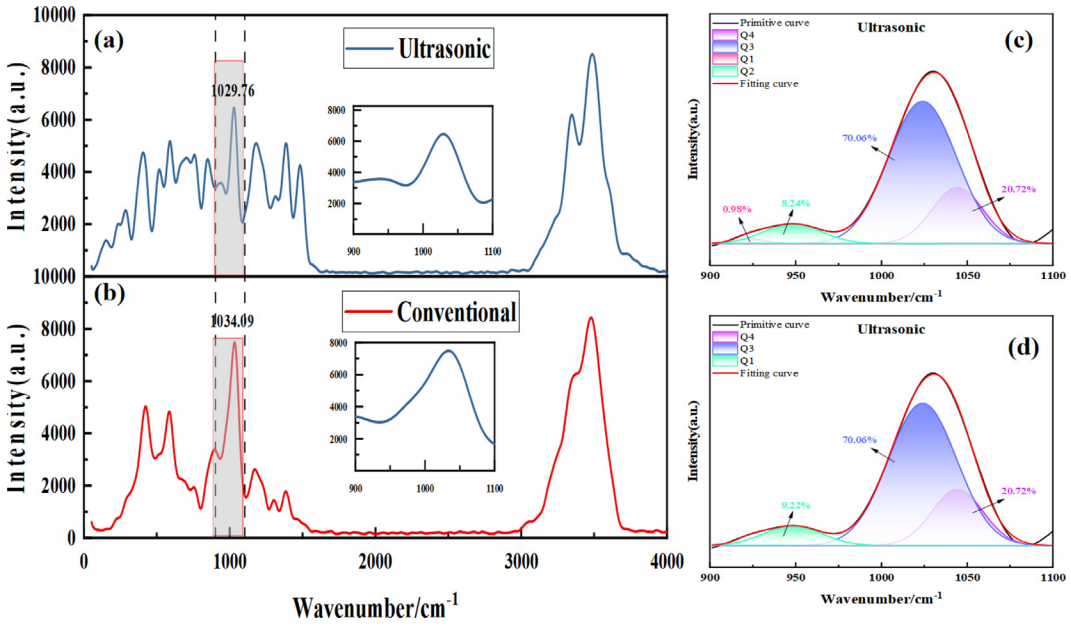

Fig. 9 Raman spectral analysis of centrifugal slag under ultrasonic and conventional conditions (a and c are Raman spectra of ultrasonic and conventional centrifugal slag respectively, b and d are Gaussian Raman spectra of ultrasonic and conventional centrifugal slag respectively).

and Q4 in the Raman spectral Gaussian diagram of ultrasonic centrifugal slag are 9.22%, 70.06% and 20.72%, respectively. This indicates that the number of bridging oxygen bonds in the silicon-oxygen tetrahedron in the silica gel is significantly reduced by introducing ultrasound during the leaching process, and the highly polymerized grid-like composite structure is gradually depolymerized, resulting in a continuous decrease in the degree of polymerization of the silica gel. The silica gel with a large volume grid structure is decomposed into a small-sized oligomeric SiO2(Zhang et al., 2021; Liu et al., 2021; Cook, 2022). In general, the adsorption capacity of long-chain polymers is higher than that of short-chain polymers. Therefore, after ultrasonic treatment, the depolymerization of silica gel is intensified, resulting in a decrease in the adsorp-

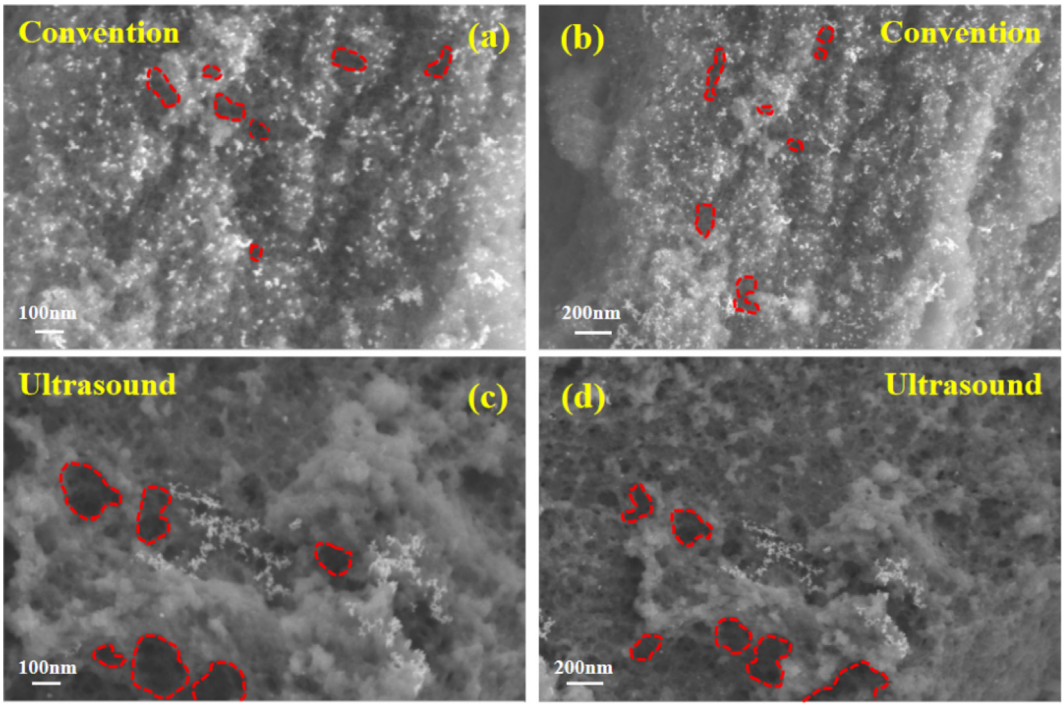

Fig. 10 SEM morphology of centrifugal slag under ultrasonic and conventional conditions.

tion capacity of silicon for germanium, thereby reducing the loss of germanium in the leaching process(Xinhao, 2022; Swedlund and Webster, 1999).

3.3.4. Comparative characterization of SEM morphology

Fig. 10 is the SEM morphology of centrifugal slag under ultrasonic and conventional conditions. It can be clearly seen from the figure that the pore size of the centrifugal slag surface under conventional conditions is small, while the pore size of the centrifugal slag under ultrasonic conditions is significantly larger than that under conventional conditions. The results of the SEM morphology are completely consistent with the above specific surface area and pore size analysis results. It can be found from the following figure that the surface of the centrifugal slag is attached to obvious white particles, which is the result of the adsorption of silicic acid colloid. Compared with the conventional conditions, the particles adsorbed on the surface of the centrifugal slag under ultrasonic conditions are greatly reduced, which is caused by the jet and cavitation effect generated by ultrasound in the solid–liquid system. The effect of ultrasound in solution is shown in Fig. 11. It can be clearly seen from Fig. 11 that ultrasonic waves produce shock waves and micro-jets in solution. In the leaching system, the mechanical effects such as micro-jet, impulse wave and acoustic flow will cause high-speed collision between liquid macroscopic turbulence and solid particles. In the solution, the velocity of acoustic flow is much faster than that of thermal convection. The acoustic flow effect will accelerate the circulation speed of the solution and make the solution vibrate violently(Lim and Shon, 2015; Xin et al., 2022). Ultrasonic action will produce cavitation bubbles in the solution. When the cavitation bubbles grow to a certain extent, the cavitation bubbles will break up, release a lot of heat in the solution and produce a local high pressure environment. Under strong oscillation and local high temperature and high pressure conditions, the silicic acid colloid will disintegrate and the germanium adsorbed on the surface of the silicic acid colloid will be peeled off.

3.4. Ultrasonic depolymerization germanium silicon precipitation mechanism

Fig. 12 is the mechanism diagram of ultrasonic depolymerization of germanium silicon precipitation. Ultrasonic waves will

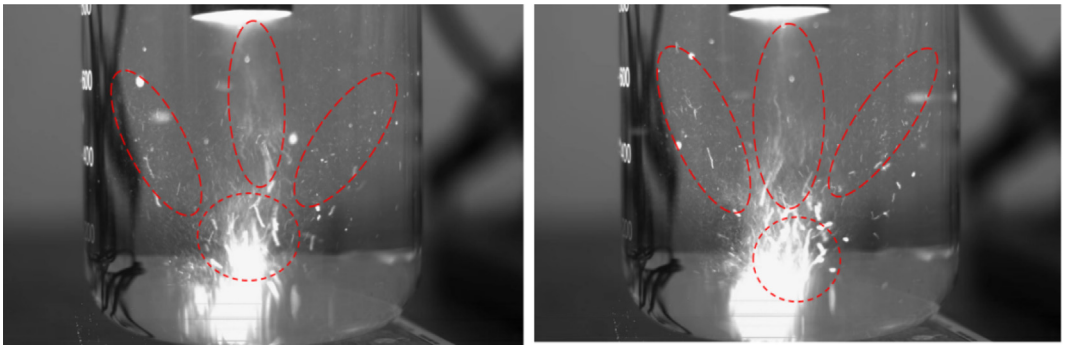

Fig. 11 Effect of ultrasound in solution.

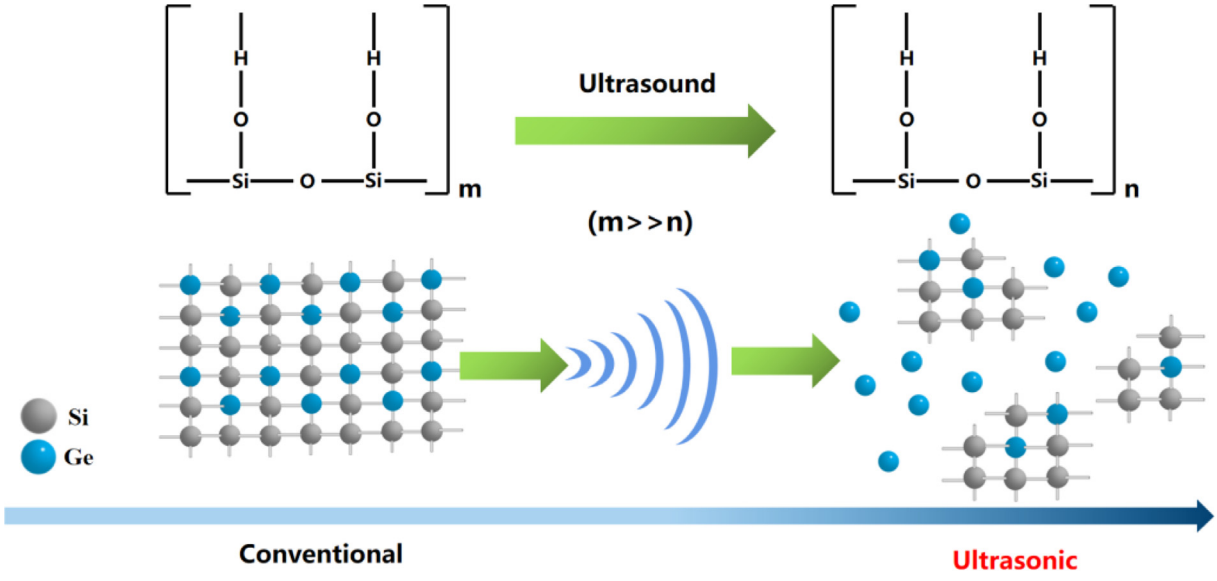

Fig. 12 Mechanism diagram of ultrasonic depolymerization of germanium silicon precipitation.

produce cavitation bubbles in the solution, and the cavitation effect will occur. The energy released when the cavitation bubbles burst will form a local high temperature and high pressure and produce shock waves and micro-jets, which will continuously impact the surface of the silica gel, making the surface pore size and pore volume of the silica gel increase. Ultrasonic waves can destroy the grid structure of silica gel, depolymerize large particles of silica gel into small particles of silicic acid molecules, promote the Co-precipitation and decomposition of silicon and germanium, reduce the adsorption of germanium by silica gel, and strip the germanium adsorbed on the surface of silica gel, thereby reducing the loss of germanium.

4. Conclusion

In this study, aiming at the loss of germanium in the leaching process of zinc oxide dust, the mechanism of polymerization and precipitation of silicon and germanium was analyzed by simulated solution experiment. The ultrasonic wave was innovatively introduced to realize the efficient dispersion and depolymerization of germanium and silicon precipitation. Research shows that:

(1) Pure solution was used to simulate the leaching process of zinc oxide dust. The results showed that the loss rate of germanium in the simulated solution was 14.81 % in the traditional leaching process, while the loss rate of germanium in the simulated solution was only 6.02 % after ultrasonic treatment, which was 59.35 % lower than the traditional process.
(2) In the leaching process of germanium-containing zinc oxide dust, due to the increase of local pH in the solution, some silicon is hydrolyzed to form silica gel, which adsorbs the germanium leached from the solution, resulting in the loss of germanium.
(3) Ultrasound was introduced during the leaching process. The cavitation effect and mechanical effect produced by ultrasound will expand the pore size and pore volume of the surface of the silicic acid colloid, the adsorbed germanium on its surface is desorbed. Moreover, ultrasound can destroy the lattice structure of silica gel, and decompose the large volume of silica gel with grid structure into small size silicic acid molecules, which aggravates the depolymerization reaction of the silica gel and reduces the adsorption capacity of silicon for germanium, thereby inhibiting the loss of germanium during the leaching process.

Compared with the methods reported above, this study has the characteristics of small equipment investment, easy connection with existing industrial production, and green environmental protection of products. And other impurity ions will not be introduced in the leaching, affecting the subsequent production process. In summary, the proposed method is economical and environmentally friendly, and has significant prospects for the efficient recovery of germanium from zinc oxide dust and the comprehensive utilization of germanium resources on an industrial scale.

Declaration of Competing Interest

The authors declare that they have no known competing financial interests or personal relationships that could have appeared to influence the work reported in this paper.

Acknowledgements

This work was supported by National Natural Science Foundation of China[grant number 51974141], Major Science and Technology Project of Yunnan Province [grant number 202202AB080005], Yunnan Fundamental Research Projects [202301AT070480], Yunnan Fundamental Research Projects [202101AT070280].

References

Bo-kang, L., Yang, L., 2007. An experimental study of the enrichment of indium and germanium via high temperature volatilization of zinc residue [J][J]. Southern Metals 3, 7–9.
Chunfu, X.I.N., Hongying, X.I.A., Libo, Z.H.A.N.G., et al, 2021. Research process on recovery and utilization of valuable metals from zinc oxide dust containing Germanium[J. Nonferrous Metals Eng. 11 (06), 66–74.
Cook, B., 2022. Silicon-Germanium: the legacy lives on[J]. Energies 15 (8), 2957.
Dass, D., 2019. Effects of surface passivation by hydrogen on the structural and electronic properties of a germanium nanowire: a sp3 tight binding study[J]. Appl. Surf. Sci. 488, 404–417.
Geng, X., Liu, Y., Zhang, W., et al, 2022. Recent advances in the recovery of germanium during the zinc refining process[J]. Chem. Eng. J., 137445
Guohua, L.I., Mingde, T.A.O., Hui, T.A.N., et al, 1987. Raman scattering from amorphous SiC and Ge-C films[J]. J. Semicond. 02, 182–185.
Harbuck, D.D., 1993. Increasing germanium extraction from hydrometallurgical zinc residues[J]. Mining, Metall. Explor. 10 (1), 1–4.
Harbuck, D.D., 1992. Gallium and germanium recovery from domestic sources[M]. US Department of the Interior, Bureau of Mines
Huang, T., Cao, Q., Jing, B., et al, 2022. Towards high-performance lithium-sulfur battery: Investigation on the capability of metalloid to regulate polysulfides[J]. Chem. Eng. J. 430, 132677.
Jadhav, S.A., Garud, H.B., Patil, A.H., et al, 2019. Recent advancements in silica nanoparticles based technologies for removal of dyes from water[J]. Colloid Interface Sci. Commun. 30, 100181.
Jikun, W.A.N.G., Aiping, H.E., 2005. Modern germanium metallurgy [M]. Metallurgical Industry Press, Beijing.
Ji-min, W., Hong-yang, C.A.O., Shao-chun, C., et al, 2014. Recovery of Ge/Ga/In from replacement slag in pressure oxidation leaching process of zinc sulfide concentrate[J]. Chinese J. Rare Metals 38 (3), 471–479.
Jordens, J., De Coker, N., Gielen, B., et al, 2015. Ultrasound precipitation of manganese carbonate: the effect of power and frequency on particle properties[J]. Ultrason. Sonochem. 26, 64–72.
Li, Z.X., Wang, C.Y., Yin, X.M., et al, 2017. Extraction of germanium and zinc from germanium-bearing zinc oxide dust[J]. Nonferrous Met. 9, 45–47.
Li, L., Zhai, L., Zhang, X., et al, 2014. Recovery of valuable metals from spent lithium-ion batteries by ultrasonic-assisted leaching process[J]. J. Power Sources 262, 380–385.
Likun, G.U., 2020. Experimental study on increasing germanium leaching efficiency from zinc oxide dust[J]. China Mining Magazine 29 (S1), 419-421, 424.
Lim, K., Shon, B., 2015. Metal components (Fe, Al, and Ti) recovery from red mud by sulfuric acid leaching assisted with ultrasonic waves[J]. Int. J. Emerg. Technol. Adv. Eng. 5 (2), 25–32.
Liu, F.P., Liu, Z.H., Li, Y.H., et al, 2016. Sulfuric leaching process of zinc powder replacement residue containing gallium and germanium[J]. Chinese J. Nonferreous Met. 26, 908–916.
Liu, F., Liu, Z., Li, Y., et al, 2016. Extraction of gallium and germanium from zinc refinery residues by pressure acid leaching[J]. Hydrometall. 164, 313–320.
Liu, F.P., Liu, Z.H., Li, Y.H., et al, 2017. Oxalic acid leaching process of zinc powder replacement residue containing gallium and germanium[J]. Chinese J. Nonferreous Met. 27 (10), 2154–2163.

Liu, C., Zhang, R., Zhao, X., et al, 2021. Quantification of phosphorus structures in CaO-SiO_2-P_2O_5 glasses via Raman spectroscopy[J]. J. Non Cryst. Solids 557, 120579.

Lu, P., Xia, W., Jiang, H., et al, 2015. Analysis of high alumina silicate glass with infrared and raman spectroscopy[J]. Bull. Chin. Ceram. Soc. 34, 878–887.

Lulu, M.A., Cuili, C.H.E.N.G., Zhenkun, L.E.I., et al, 2016. Experimental analysis for residual stress inside biaxial strained silicon material with Germanium silicon buffers (ε-Si/$Ge_{0.3}Si_{0.7}$/Ge_xSi_{1-x}/C-Si) by using Micro-Raman[J]. J. Exp. Mech. 31 (03), 306–314.

Marek, P.L., 2013. Biomimetic dye aggregate solar cells[M]. Springer Science & Business Media.

Markus, H., Fugleberg, S., Valtakari, D., et al, 2004. Reduction of ferric to ferrous with sphalerite concentrate, kinetic modelling[J]. Hydrometall. 73 (3–4), 269–282.

Miao, D., 2020. Study and application of hydration characteristics of layered sodium silicate-silica fume-cement slurry[D]. Chengdu: Chengdu University of Technology DOI:10.26986/d.cnki.gcdlc.2020.000212.

Mochida, N., Sakai, K., Kikuchi, K., 1984. Raman spectroscopic study of the structure of the binary alkali germanate glasses[J]. J. Ceram. Ass., Japan 92 (1064), 164–172.

Patil, V.L., Vanalakar, S.A., Tarwal, N.L., et al, 2019. Construction of Cu doped ZnO nanorods by chemical method for Low temperature detection of NO2 gas[J]. Sens. Actuators, A: Phys. 299, 111611.

Rouchon, D., Mermoux, M., Bertin, F., et al, 2014. Germanium content and strain in $Si_{1-x}Ge_x$ alloys characterized by Raman spectroscopy[J]. J. Cryst. Growth 392, 66–73.

Song, L., Di, H., Yang, K., et al, 2022. Ultrasonic-enhanced sulfuric acid leaching kinetics of high-grade germanium-containing materials[J]. Chem. Eng. Process.-Process Intensif. 178, 109045.

Sutar, S.S., Patil, S.M., Kadam, S.J., et al, 2021. Analysis and prediction of hydrothermally synthesized ZnO-based dye-sensitized solar cell properties using statistical and machine-learning techniques[J]. ACS Omega 6 (44), 29982–29992.

Swedlund, P.J., Webster, J.G., 1999. Adsorption and polymerisation of silicic acid on ferrihydrite, and its effect on arsenic adsorption[J]. Water Res. 33 (16), 3413–3422.

Tan, J., Zhao, S., Wang, W., et al, 2004. The effect of cooling rate on the structure of sodium silicate glass[J]. Mater. Sci. Eng. B 106 (3), 295–299.

Tarwal, N.L., Mali, D.P., Patil, K.V., et al, 2023. Spray deposition of the nanostructured ZnO thin films for non-volatile resistive switching memory applications[J]. Appl. Phys. A 129 (1), 1–12.

Ting, L., Xuan, L., Yanfei, Z., et al, 2015. Development strategies for the Chinese indium, germanium and gallium industry based industry chain analysis[J]. Resour. Sci. 37, 1008–1017.

Verweij, H., Buster, J., 1979. The structure of lithium, sodium and potassium germanate glasses, studied by Raman scattering[J]. J. Non Cryst. Solids 34 (1), 81–99.

Wang, S., Cui, W., Zhang, G., et al, 2017. Ultra fast ultrasound-assisted decopperization from copper anode slime[J]. Ultrason. Sonochem. 36, 20–26.

Wang, W., Wang, F., Lang, J., 2017. Recovery germanium by microwave alkaline roasting-water dissolving from zinc oxide dust bearing germanium[J]. Conserv. Utiliz. Miner. Resour. 6, 26–31.

Xiaodong, Z., Feiyan, Z., 2018. Application of metal germanium in high-tech field[J]. Coal and Chemical Industry (2), 32-34.

Xin, C., Xia, H., Jiang, G., et al, 2022. Mechanism and kinetics study on ultrasonic combined with oxygen enhanced leaching of zinc and germanium from germanium-containing slag dust[J]. Sep. Purif. Technol. 302, 122167.

Xinhao, H., 2022. Characteristics and Mechanism of Extracting Germanium from Low Germanium Bearing Residue with High Silicon Content[D]. Jiangxi: Jiangxi University of Science and Technology. DOI:10.27176/d.cnki.gnfyc.2022.000581.

Xu, Y., Xia, H., Zhang, Q., et al, 2023. Ultrasonic enhanced hydrazine sulfate acid leaching of low-grade germanium dust[J]. Appl. Energy 332, 120485.

Yan, J.W., Pan, D.A., Li, B., 2020. Application of ultrasonic intensification in hydrometallurgy leaching process[J]. Chin. J. Process Eng. 20, 1–7.

Yanlin, L., Zhigan, D., Yingxu, Z., et al., 2021. Study on Leaching of Zn and Ge from Ge-bearing Zinc Oxide Dust[J]. Nonferrous Metals(Extractive Metallurgy) (07), 49-54 + 69.

Yingxu, Z., Zhigan, D., Chang, W., et al, 2021. Leaching germanium-containing zinc oxide dust by atmospheric oxygen enrichment[J]. Chinese J. Nonferrous Met. 31 (4), 995–1006.

Zhang, T., Jiang, T., Liu, Z., 2019. Recovery of Ge (IV) from synthetic leaching solution of secondary zinc oxide by solvent extraction using tertiary amine (N235) as extractant and trioctyl phosphate (TOP) as modifier[J]. Miner. Eng. 136, 155–160.

Zhang, Y.X., Li, H.R., Liu, S.Y., et al, 2021. Raman spectroscopic study of irregular network in the process of glass conversion to CaO-MgO-Al_2O_3-SiO_2 glass-ceramics[J]. J. Non Cryst. Solids 563, 120701.

Zhang, L., Song, Q., Xu, Z., 2018. Thermodynamics, kinetics model, and reaction mechanism of low-vacuum phosphate reduction process for germanium recovery from optical fiber scraps[J]. ACS Sustain. Chem. Eng. 7 (2), 2176–2186.

Zhang, R., Wang, Z., Meng, Y., et al, 2021. Quantitative insight into aluminum structures in CaO-Al_2O_3-SiO_2 system via Raman and 27Al MAS-NMR spectroscopies[J]. J. Non Cryst. Solids 573, 121116.

Zhang, R.L., Zhang, X.F., Tang, S.Z., et al, 2015. Ultrasound-assisted HCl–NaCl leaching of lead-rich and antimony-rich oxidizing slag [J]. Ultrason. Sonochem. 27, 187–191.

Zhaohui, L., Xiao, W., Yongding, H., et al, 2010. Relevant research on disposal of municipal sludge by ultrasonic wave[J]. Environ. Sci. Tech. 23 (04), 69–72.

Zhengwei, S., Shuhui, C., Jingwen, Z., 2015. Current situation and sustainable development suggestions of Germanium resources in China[J]. Mining Res. Development 35 (11), 108–112.

Zhigan, D., Yingxu, Z., Chang, W., et al, 2020. Recovery of zinc and germanium from zinc oxide dust containing germanium by atmospheric oxygen enrichment leaching[J]. Mining Metall. 29 (01), 37–43.